scientific reports

Check for updates

OPEN

Human lncRNAs NEAT1 and MALAT1 regulate the tumor microenvironment in lung cancer PDX models in athymic nude mice

Min-Shiau Hsieh[1,3,5], Meng-Xian Lin[2,5], Bing-Ying Ho[2,4]✉ & Jong-Kai Hsiao[2,3]✉

We employed PDX models in athymic nude mice to generate lung cancer tumors, aiming to improve early detection and enable personalized treatments. The athymic nude mouse was utilized as the lung cancer PDX model, maintaining the histological and pathological integrity of lung cancer. This model allowed for the analysis of microenvironments through whole transcriptome sequencing to assess gene expression variations across different passages of the PDX model. Candidate genes identified from the RNA-seq analysis were subsequently verified using RT-qPCR. We identified significant changes in genes related to tumor adaptation and immune interactions. Notably, there was a decrease in the expression of *Eat-2*, *Itgb2*, *Klrd1*, and *Nkg2d*, which are important for NK cell cytotoxic activity. This decrease correlated with the reduction in tumor growth rate from P0 (248 days) to P3 (69 days) to achieve the same tumor volume. Additionally, a decline in the lncRNAs NEAT1 and MALAT1 from PDX passage P0 to P3 was observed and impacting NK cell function and suggesting significant immune system involvement in tumor growth and engraftment. Our findings demonstrate the value of the PDX athymic mice model in lung cancer research. These models are essential for exploring tumor-immune dynamics and developing tailored therapeutic approaches, providing significant insights into tumor behavior and treatment responses.

Keywords PDX, NK cells, MALAT1, NEAT1

Lung cancer remains the leading cause of cancer-related mortality worldwide, representing a significant global health challenge[1]. Despite advances in early detection and therapeutic strategies, the development of novel approaches is imperative for improving patient outcomes. Recent investments in targeted lung cancer interventions have led to measurable reductions in mortality rates[1,2]. In this evolving landscape, patient-derived xenograft (PDX) models have gained prominence in translational cancer research, which facilitate the evaluation of precision treatments, enable personalized medicine strategies, and enhance the predictive accuracy of clinical trial drug responses[3,4].

PDX models are particularly valued for their ability to mimic the human tumor microenvironment within an animal host, preserving tumor heterogeneity, histopathological characteristics, and critical stromal elements of lung cancer[5–7]. Various types of immunodeficient mice, including athymic nude, NOD-SCID, and NSG mice, have been employed to establish lung cancer PDX models, each offering different levels of engraftment success and utility[8,9]. Despite the limitation of immune response activity, the use of athymic nude mice remains prevalent, particularly for their compatibility with imaging-assisted co-clinical trials[10]. To enhance the translational relevance of these models, our study aims to dissect the molecular mechanisms that influence the engraftment and growth of human tumor tissues in these hosts.

This research undertakes a novel comparison of gene expression profiles at various stages of PDX model development from the same tumor lesion. By analyzing these stage-specific changes, we aim to uncover molecular dynamics that could affect tumor growth. Our findings offer new insights into the behavior of human lung tumors in athymic nude mice, contributing valuable perspectives to the field of lung cancer research.

[1]Division of Thoracic Surgery, Department of Surgery, Taipei Tzu Chi Hospital, Buddhist Tzu Chi Medical Foundation, New Taipei City 23142, Taiwan. [2]Department of Medical Imaging, Taipei Tzu Chi General Hospital, Buddhist Tzu-Chi Medical Foundation, New Taipei City 23142, Taiwan. [3]School of Medicine, Tzu Chi University, Hualien 97004, Taiwan. [4]Molecular Imaging Center, National Taiwan University, Taipei 10672, Taiwan. [5]Min-Shiau Hsieh and Meng-Xian Lin contributed equally to this work. ✉email: beingho@gmail.com; jongkai@tzuchi.com.tw

Materials and methods

Clinical tumor samples collection

Tumor specimens were obtained from lung cancer patients who underwent surgical procedures at Taipei Tzu Chi General Hospital, Taiwan. The collection and use of these specimens were conducted in accordance with a study protocol that received independent approval from the Institutional Review Board (IRB) of Taipei Tzu Chi General Hospital, Buddhist Tzu Chi Medical Foundation (IRB approval number: 10-XD-104). Informed consent was given by all patients. During collection, care was taken to select the most representative sections of the tumor foci. Tissue from central liquefied or necrotic parts of the tumor was avoided. Selected tissues were dissected into small pieces, approximately 0.5 cm x 0.5 cm x 0.5 cm each, and immediately placed in centrifuge tubes filled with phosphate-buffered saline (PBS). These samples were then stored in an ice bath, ready for subsequent processing and PDX model passage.

Animals

BALB/cAnN.Cg-Foxnlnu/CrlNarl athymic nude mice, aged 6–8 weeks, were acquired from the National Laboratory Animal Center, Taiwan. These mice were specifically chosen for this study based on their suitability for experimental purposes. All experimental procedures involving these mice were conducted in strict accordance with the guidelines set forth by the Institutional Animal Care and Use Committee (IACUC) of Taipei Tzu Chi General Hospital, Buddhist Tzu Chi Medical Foundation, under approval number 110-IACUC-016.

PDX model generation

Mice were anesthetized using isoflurane (AbbVie Global, Taipei, Taiwan) at a 2% concentration with an oxygen flow rate of 1 L/minute, administered via a nose cone. Fresh tumor specimens were sectioned into fragments approximately 3–5 mm^2 in size and immersed in PBS containing Penicillin/Streptomycin antibiotics. Each fragment was then carefully coated in Matrigel before being surgically implanted subcutaneously into the lower backs of 6–8 week old nude mice. The PDX tumors used in this experiment reached a target volume of approximately 2000 mm^2, with radii measuring between 10 and 13 mm, at which point they were harvested under sterile conditions. Mice were anesthetized, and tumors were completely excised. These tumors were then processed using the initial model construction method and transplanted into a new passage of nude mice for further growth. The process was repeated until the fourth passage (P0 to P4), at which point the PDX models demonstrated successful engraftment. For each series of P0-P4 grafts, tumor samples from athymic nude mice ($N = 1$ for each passage) were subsequently harvested, frozen, and stored for future research.

Whole-transcriptome sequencing and analysis

We use DESeq v1.38.0,A basic task in the analysis of count data from RNA-seq is the detection of differentially expressed genes. The package DESeq provides methods to test for differential expression; the estimates of dispersion and logarithmic fold changes incorporate data-driven prior distributions. Total RNA was prepared using the Illumina TruSeq Stranded Total RNA Library Prep Gold Kit (Illumina, San Diego, USA), following a ribosomal RNA depletion step as per the manufacturer's instructions. RNA purity and concentration were assessed using a ND-1000 spectrophotometer (Nanodrop Technologies, USA) at OD260 nm, while RNA integrity was evaluated with a Bioanalyzer 2100 (Agilent Technologies, USA) employing the RNA 6000 Nano kit.

Library construction was performed using the same Illumina kit (Cat. No. 20020598), and libraries were size-selected using AMPure XP beads (Beckman Coulter, USA). Sequencing was conducted on an Illumina HiSeq 4000 system (LC Bio, China) using Illumina's sequencing-by-synthesis (SBS) technology. This process generated paired-end sequencing data, which were then converted from bcl to FASTQ format using Welgene Biotech's pipeline based on the Illumina basecalling software bcl2fastq version 2.20 (WELGENE, Taiwan).

Human (GRCh38) and mouse (GRCm38) were used as reference genome for mapping, respectively. The standard analysis pipeline for RNA sequencing contains three parts of secondary analysis: Differential Expression Gene (DEG) analysis, and Enrichment Analysis. We import the outcomes from the software — "HISAT2 v2.2.1" and "StringTie v2.1.7", and perform advanced analyses with third-party packages, such as DESeq v1.38.0 and clusterProfiler v4.7.1. Quantitative analysis of the transcriptome data was carried out using Hisat2 and StringTie software, with differential expression analysis conducted in R using the Ballgown package. Both upregulated and downregulated genes, with a log2 fold change of ≥ 2 and a false discovery rate (FDR) of ≤ 0.05, are now considered in our analysis to ensure a comprehensive evaluation of gene expression changes.

RT-qPCR analysis

Total RNA was extracted using TRIzol reagent (Invitrogen) according to the manufacturer's instructions. The expression profiles of human long non-coding RNAs (lncRNAs) MALAT1 and NEAT1, murine lncRNAs malat1 and neat1, and the murine transcript RNA itgb2 were analyzed by quantitative real-time PCR (RT-qPCR). These assays were conducted using the StepOnePlus Real-Time PCR System (Thermo Fisher Scientific, USA). Glyceraldehyde 3-phosphate dehydrogenase (GAPDH) was employed as the reference gene for both human and murine samples. Each RT-qPCR reaction was set up in a total volume of 50 µL, including 0.5 µg of total RNA, 100 nM of each primer (Table 1), and reagents from the 1Step RT PCR Kit (HighQu, Germany). The relative expression levels of the target genes were quantified using the $2-\Delta\Delta Ct$ method. All measurements were performed in triplicate to ensure reproducibility.

Gene ontology (GO) and pathway analysis

To investigate functional enrichments among the differentially expressed genes, Gene Ontology (GO) and pathway analyses were conducted using the Database for Annotation, Visualization, and Integrated Discovery

Target RNA	Sequences	Direction	Product size (bp)
Human MALAT1	5'-CTTCCCTAGGGGATTTCAGG-3'	Forward	76
	5'-GCCCACAGGAACAAGTCCTA-3'	Reverse	
Human NEAT1	5'-CTTCCTCCCTTTAACTTATCCATTCAC-3'	Forward	116
	5'-CTCTTCCTCCACCATTACCAACAATAC-3'	Reverse	
Human GAPDH	5'-CGACCACTTTGTCAAGCTCA-3'	Forward	163
	5'-CCCTGTTGCTGTAGCCAAAT-3'	Reverse	
Murine Malat1	5'-TCTTCTATTCTTCGGCTTCCTACT-3'	Forward	66
	5'-AAGCATCTTTAGAAGACAGAAAAG-3'	Reverse	
Murine Neat1	5'-TGTTAAAGGCGCTTTGGAAG-3'	Forward	76
	5'-GCGGGGCTAAGTATAAAGGAG-3'	Reverse	
Murine Itgb2	5'-AGCAGAAGGACGGAAGGAACATTTAC-3'	Forward	136
	5'-ATGACCAGGAGGAGGACACCAATC-3'	Reverse	
Murine Klrd1	5'-AGCCTTCTTCAGCCCCAATC-3'	Forward	201
	5'-AACGCTTTTGCTTGGACTGT-3'	Reverse	
Murine Nkg2d	5'-TGGCTTGCCATTTTCAAAGAGAC-3'	Forward	95
	5'-TTAGGGCATGGGCCACAGTA-3'	Reverse	
Murine Eat-2	5'-TTTGTTCCCCGCAGGCTTC-3'	Forward	146
	5'-CGCATGGGACTCACAGAACT-3'	Reverse	
Murine Gapdh	5'-CTGGAGAAACCTGCCAAGTAT-3'	Forward	125
	5'-GAGTTGCTGTTGAAGTCGCAG-3'	Reverse	

Table 1. Sequences of primers used in this study.

(DAVID) online tools (version 6.8). For all analyses, a false discovery rate (FDR) threshold of 0.05 was applied to identify statistically significant enrichments.

To visually represent the most significantly enriched GO terms and pathways, a word cloud was generated. This visualization was created using the 'wordcloud' package in R (version 2.6), provided by WELGENE, Taiwan. The size of each term in the word cloud is proportional to the -log10 (p-value) of the enrichment, highlighting the terms with greater significance.

Immunofluorescence staining

Tissue sections were fixed overnight in 4% paraformaldehyde, followed by paraffin embedding. Sections with a thickness of 5-μm were prepared for histological examination and stained with hematoxylin and eosin for routine immunohistochemical analysis. For immunofluorescence, additional slices of 5-μm thickness were fixed in cold acetone for 10 min and then air-dried for 30 min. After rinsing with PBS, sections were blocked using a 10% blocking buffer for 30 min at room temperature. The slides were then incubated with an NK cell-specific marker (ANK61, sc-59340, Santa Cruz Biotechnology) followed by conjugation with Alexa Fluor 488-labeled secondary antibodies (MAB2300X, Sigma-Aldrich) for indirect immunofluorescence staining. Nuclei were stained with 4',6-diamidino-2-phenylindole (DAPI, Santa Cruz Biotechnology). Fluorescence images were acquired using a BX43 microscope equipped with a DP80 microscope digital camera (Olympus).

Results

PDX model generation

Among the included ten clinical lung cancer patients, only case (#7) representative lung cancer tumor case was successfully established in the PDX model (L7 PDX) by nude mice, and they were passed from P0–P4 generations. While observing L7 PDX models, we found that tumor growth in P0 was slow in the early stage after transplantation. However, the tumor growth rate accelerated significantly as time progressed. We document the establishment process of the PDX model for this lung cancer case for subsequent transplantation into the next cohort of mice. The time required for PDX passage from P0 to P4 is 248, 111, 78, 69, and 78 days, respectively. We found that the tumor formation time decreased dramatically with the number of passages (Fig. 1). We suppose that the human tumor transplant to nude mice at P0 in the early stage would make a significant impact on the host. Although nude mice lack a thymus, they still have some immune defense functions, such as NK or macrophages, to defend against foreign infiltration. Meanwhile, P1-P4 reduced the duration required for PDX passage, whereas P0 necessitates an extended period to adapt to the foreign tissue transplanted through clinical surgery. Histological examination of tumor sections stained with Haematoxylin Eosin (HE) revealed that the lung PDX margins displayed a high nuclear to cytoplasmic ratio, large hyperchromatic nuclei, and occasional prominent nucleoli (Fig. 2).

Identification of gene expression changes association with Po and P3

In this study, human (GRCh38) and mouse (GRCm38) reference genomes were used for mapping, respectively. We analyzed a total of 11,073 and 25,554 variables in human and mouse genes, respectively. We identified a total of 3 upregulated and 136 downregulated DEGs in human genes, and 361 upregulated and 637 downregulated

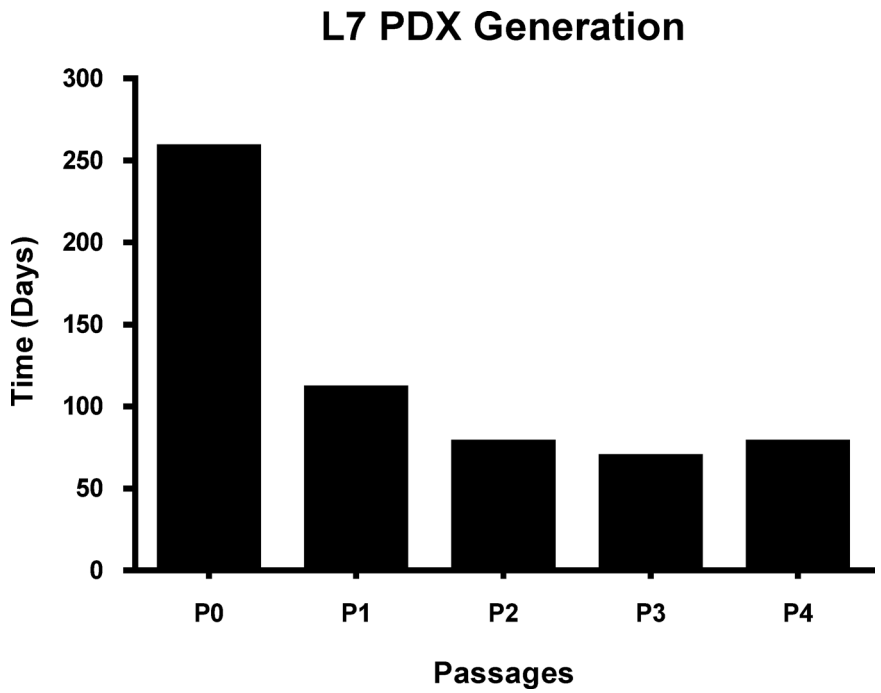

Fig. 1. Tumor formation rate over successive passages in L7 PDX models. Subsequent passages (P1 to P4) demonstrate a significant decrease in the time required for tumor formation, indicating an adaptation process that facilitates faster tumor growth in later passages.

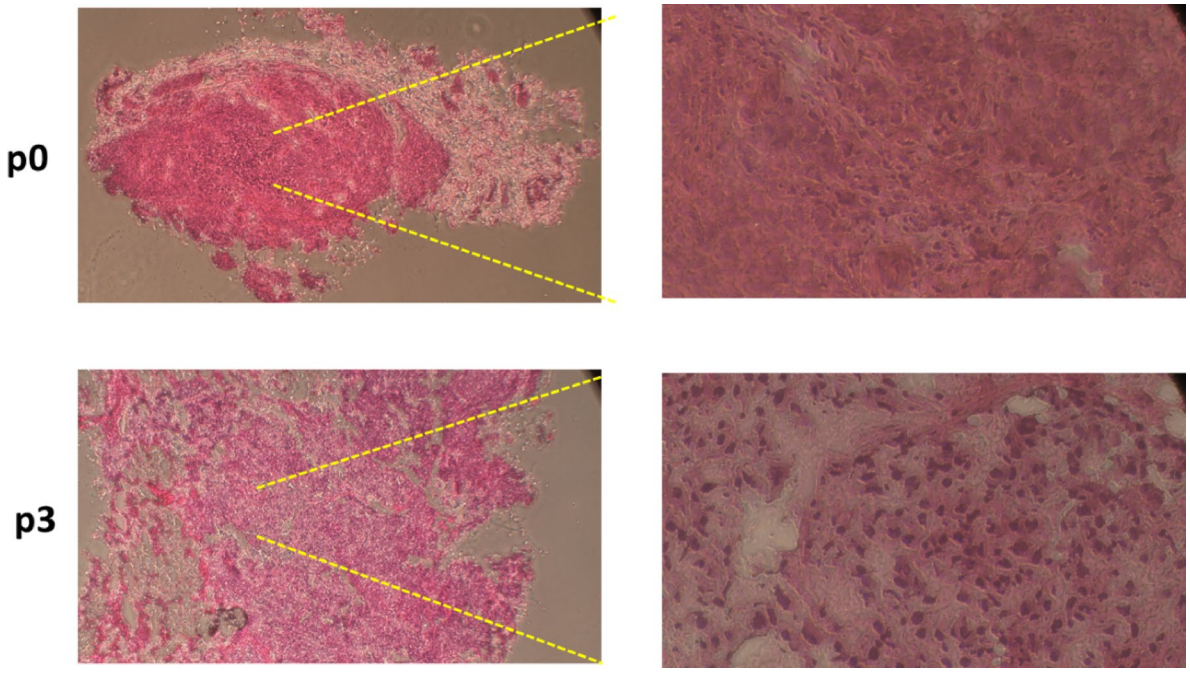

Fig. 2. PDX tumor HE staining from different passages. Malignant cells exhibit a high nuclear to cytoplasmic ratio, large hyperchromatic nuclei, and occasional prominent nucleoli. Images are shown at a magnification of ×40 in the right panel.

DEGs in mouse genes. The volcano plots revealed the distribution of DEGs in both human and mouse genes, demonstrating the patterns of upregulation and downregulation of distinct genes between the P0 and P3 passages (Fig. 3).

Gene ontology analysis was performed by using the DAVID online tools[11]. Enriched GO terms were grouped in the three categories: enrichment molecular function (MF), biological process (BP), and cellular component (CC), respectively. In the enrichment MF category, 12 terms were significantly enriched ($p < 0.05$), including structural constituent of ribosome, ATP-dependent activity, acting on DNA, helicase activity, catalytic activity acting on DNA, protease binding, hormone activity, GTPase regulator activity, nucleoside-triphosphatase regulator activity, cytokine receptor binding, cytokine activity, ion channel regulator activity, and phosphoprotein binding. The 11 enriched GO terms under the enrichment BP category ($p < 0.05$) were B cell activation, neuron migration, B cell proliferation, adaptive immune response, regulation of B cell activation, activation of immune response, immune response-regulating cell surface receptor signaling pathway, immune response-activating cell surface receptor signaling pathway, immune response-activating signal transduction, T cell receptor signaling pathway, and antigen receptor-mediated signaling pathway. With respect to the enrichment CC category, 24 terms were significantly enriched ($p < 0.05$), including ribosomal subunit, large ribosomal subunit, intermediate filament, condensed chromosome, kinetochore, condensed chromosome, centromeric region, intermediate filament cytoskeleton, ribosome, mitochondrial matrix, mitochondrial protein-containing complex, nuclear chromosome, chromosomal region, inner mitochondrial membrane protein complex, contractile fiber, chromosome, centromeric region, chromosome, telomeric region, myofibril, cullin-RING ubiquitin ligase complex, extrinsic component of membrane, endosome membrane, Lamellipodium, adherens junction, collagen-containing extracellular matrix, and external side of plasma membrane. We also performed the classification of the non-redundant unigenes based on the Kyoto Encyclopedia of Genes and Genomes (KEGG) pathway[12–14] using the DAVID online tools. Fifteen KEGG pathways were significantly enriched ($p < 0.05$), including the NK cell-mediated cytotoxicity pathway (Table 2).

NK cells are lymphocytes of the innate immune system that are involved in early defenses against both allogeneic cells and autologous cells undergoing various forms of stress, such as infection with viruses, bacteria, or malignant transformation. The function of NK cells involved in tumor recognition is that they express members of the leukocyte β2 integrin family in nude mice. The requirement for β2 integrins for target-cell recognition and subsequent lysis has been described by previous studies in cytotoxic T lymphocytes and NK cells[15]. In our PDX lung cancer model, we found the expression of NK cell cytotoxic activity genes in mice, including EWS/FLI1 activated transcript 2 (*Eat-2*), integrin beta 2 (*Itgb2*), killer cell lectin like receptor D1 (*Klrd1*), and natural killer group 2 member D (*Nkg2d*), significantly decreased. These decreases were correlated with the results of the KEGG analysis and PDX tumor formation (Fig. 4).

Immunofluorescence reveals differential localization of intratumoral NK cells in p0 and p3

Our gene expression analysis indicated that NK cell-mediated cytotoxicity might influence the growth of PDX tumors (Fig. 4). To validate these findings with direct imaging evidence, we utilized an NK cell marker (ANK61) to perform immunostaining on lung cancer PDX tumor sections derived from initial clinical resections (p0) and third passage (p3) PDX models. The results from fluorescence immunostaining demonstrated a greater infiltration of NK cells in the p0 sections compared to the p3 sections. This suggests that NK cell infiltration decreases significantly after several generational passages in the lung cancer PDX model, corroborating our previous observations that the time required for tumors to reach a specified volume is substantially shortened in the PDX model after passages compared to p0 (Fig. 1).

Significant KEGG pathways identified in the human lung cancer PDX models suggest that NK cell-mediated cytotoxicity may play a crucial role in mediating the establishment of lung cancer PDX (Table 2). The presence

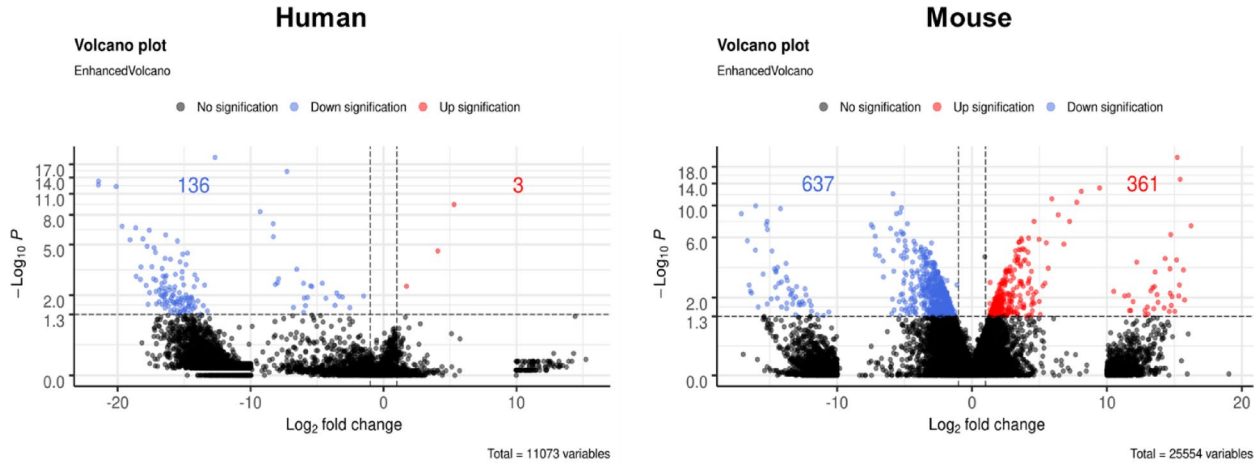

Fig. 3. Volcano plot analysis of differentially expressed genes. Upregulated (red dots) and downregulated (blue dots) genes comparing P0 and P3 (log2 fold change of ≥ 2). Non-significantly expressed genes are shown as black dots. Each dot represents one gene.

KEGG term	Enrichment score	NES
Ribosome	0.6194	1.669191
Oxidative phosphorylation	0.521	1.396706
Spliceosome	0.5209	1.39273
Staphylococcus aureus infection	0.5252	1.391516
Cell cycle	0.495	1.363818
Motor proteins	0.4552	1.275927
Neuroactive ligand-receptor interaction	0.4172	1.251523
Cytokine-cytokine receptor interaction	− 0.4927	− 1.30625
Focal adhesion	− 0.5105	− 1.312775
Relaxin signaling pathway	− 0.5345	− 1.314928
NF-kappa B signaling pathway	− 0.5703	− 1.361219
Chemokine signaling pathway	− 0.5309	− 1.361892
Natural killer cell mediated cytotoxicity	− 0.607	− 1.459652
Th17 cell differentiation	− 0.617	− 1.472817
T cell receptor signaling pathway	− 0.6728	− 1.631783

Table 2. Significant KEGG pathways of human lung cancer PDX passage (P0 versus P3). Enrichment score is represented as − log10 (p-value). The higher the enrichment score, the more significant the pathway. NES (normalized enrichment score) values indicate elevated expression (positive) and under-expression (negative) in PDX passage (P0 versus P3).

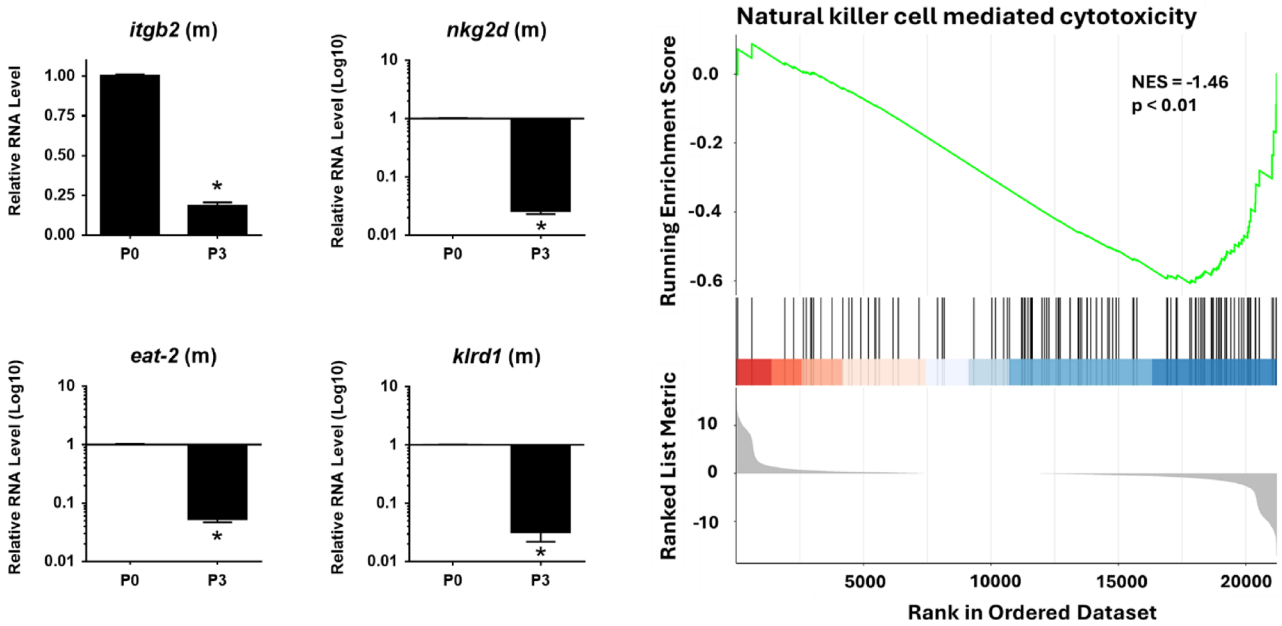

Fig. 4. Impact of NK cell-mediated cytotoxicity on PDX tumor formation. The left part of the bar graph demonstrates the association between NK cell-mediated cytotoxicity and PDX tumor formation, highlighting a significant decrease in gene expression critical for NK cell cytotoxic activity, as determined by RT-qPCR analysis. The right side of the graph displays results from KEGG pathway analysis, showing downregulation of NK cell-mediated cytotoxicity in p3 compared to p0 PDX model. Statistical analyses were performed using Student's t-test. Mean ± SEM. $^{*}p < 0.05$.

of NK cells is essential for the disruption of tumor growth in athymic nude mice. However, immunofluorescence microscopy revealed that most NK cells were localized within the tumor mass in p0. In contrast, in p3, only a small fraction of NK cells were observed infiltrating the area surrounding the tumor (Fig. 5).

Identification of LncRNA expression changes associated with PDX passage time in mice

PDX passage in nude mice is analogous to a response to stimuli, similar to bacterial or viral infection. In response to these stimuli, immune cells migrate to the transplantation site to initiate treatment. According to our RNA-seq results, we found that MALAT1 and NEAT1 act as the import roles in the NK cell-mediated pathway.

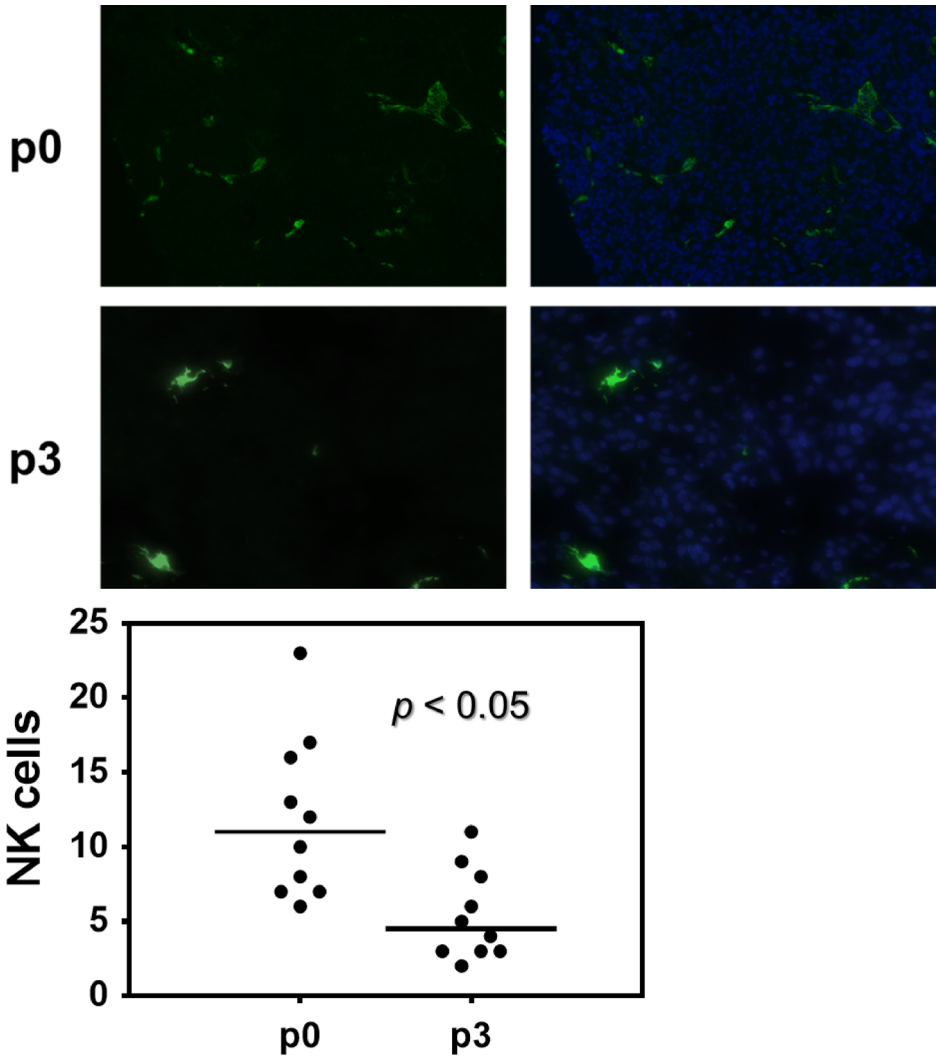

Fig. 5. NK cell density in p0 and p3 lung cancer PDX models. Green fluorescence indicates staining for NK cells, while blue fluorescence represents DAPI staining for nuclei. The analysis involved counting NK cells under a 10x microscopic field across ten different images, revealing a statistically significant difference ($p < 0.05$) between p0 and p3.

MALAT1, also known as nuclear-enriched abundant transcript 2 (NEAT2) is a large, infrequently spliced non-coding RNA that is highly conserved among mammals and highly expressed in the nucleus. Both MALAT1 and NEAT1 are highly conserved lncRNAs, found to be cancer-related and immune-specific, and are abundant in many cancer types.

RT-qPCR results indicate a significant downregulation of the human NEAT1 and MALAT1 genes from P0 to P3. The PDX microenvironment showed a substantial presence of mouse stromal cells. The mouse Neat1 gene exhibited significant downregulation from P0 to P3 ($p < 0.05$), whereas the expression of the mouse Malat1 gene did not show a significant change (Fig. 6). Human NEAT1 and MALAT1 noncoding RNAs have been described as NK cell activity inhibition. Studies have shown that NEAT1 and MALAT1 can play a role in immune modulation, particularly in promoting immune escape mechanisms in cancer cells by affecting NK cell function[16,17]. In the PDX model, which incorporates both mouse host stromal and immune cell environments, the activity of NK cells in nude mice is crucial in determining cancer growth dynamics. Previous research has indicated that extracellular vesicles serve as cargo for transporting lncRNAs to various cells[17]. We hypothesize that human lncRNAs NEAT1 and MALAT1 may be transported by extracellular vesicles, such as exosomes, to mediate the cytotoxic activity of the host's NK cells.

Discussion

In the present study, we successfully established one PDX model from 10 lung cancer patients using athymic nude mice. Among these cases, we attempted to identify potential pathological and gene expression factors that could explain the low success rate of PDX model establishment (see Supplementary Data), but no obvious indicators were found. Lung cancer case #7, characterized as T4N2M1 with pleural metastasis adenocarcinoma,

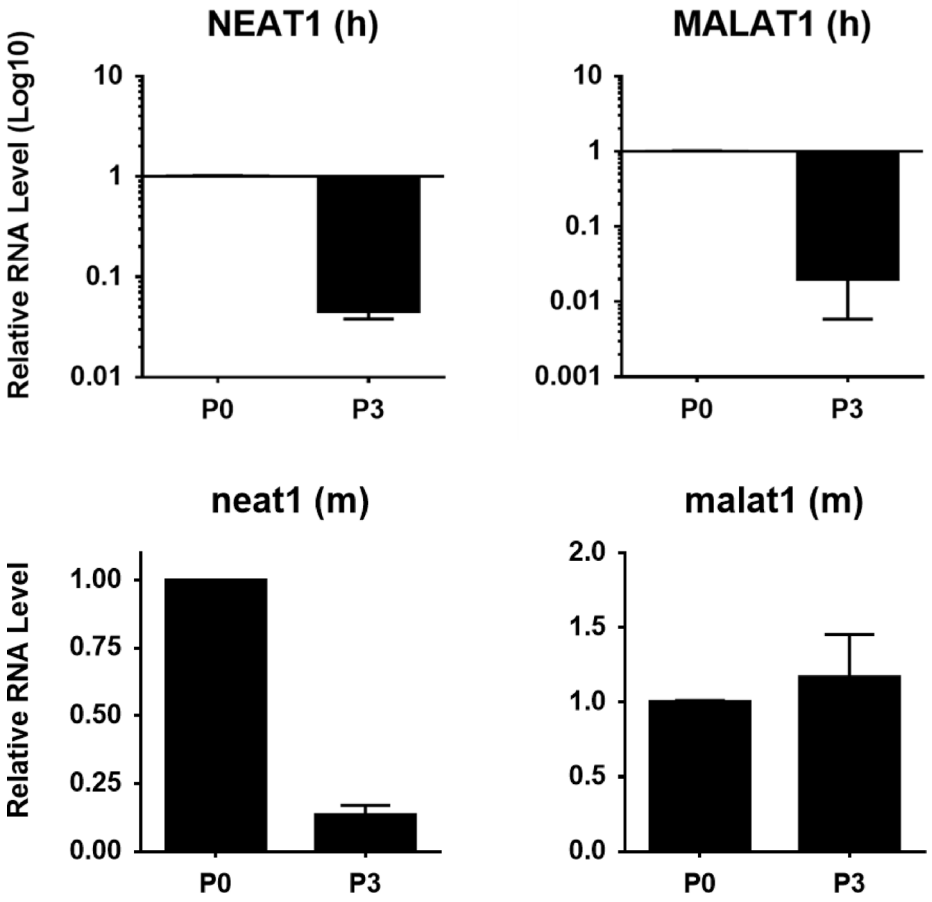

Fig. 6. RT-qPCR analysis of lncRNA expression during PDX passage P0 to P3. The dramatic downregulation of human NEAT1 and MALAT1 in the tumor tissues from the initial to later PDX passages. In contrast, murine malat1 shows relatively stable expression levels, while murine neat1 is also downregulated from P0 to P3. Statistical analyses were performed with Student's t test. Mean ± SEM. * $p < 0.05$.

did not present any particularly surprising tumor biological markers compared to other cases. The study involving the 10 cases and subsequent attempts at establishing PDX models spanned over three years. We must acknowledge the challenges encountered in this research. Consequently, we utilized RNA-seq analysis to derive insights that could not be gleaned from clinical pathological data alone. This low success rate may be attributed to the variability in host immune response activity, particularly the function of NK cells. NK cells in athymic nude mice, although partially functional, can recognize and kill transplanted tumor cells, especially during the initial passages. Tumors that can evade NK cell-mediated cytotoxicity are more likely to establish and grow in the host. Despite the relatively small sample size, we observed significant phenomena during the PDX model passage. Notably, the times required to establish the PDX models correlated with the cytotoxic activity pathway of the host's NK cells. Furthermore, the lncRNAs NEAT1 and MALAT1 within the ceRNA network played crucial roles in host immune regulation, significantly influencing tumor generation have been described[18].

PDX models are established by transplanting fresh tumor tissue resected from human cancer into mice, which provides a translational platform for testing personalized medicine approaches tailored to individual patients' tumor profiles[4]. By using PDX models derived from patient tumors, we can assess the efficacy of targeted therapies or immunotherapies in a preclinical setting, helping to predict patient responses and optimize treatment regimens before clinical implementation. This approach holds promise for advancing precision oncology and improving patient outcomes by matching treatments to the unique molecular characteristics of each patient's cancer. In our study, the tumor growth rate of P0 at 248 days was slower than that of P1 at 111 days, and the growth rate continued to decrease to 78 days at the P2 passage. Finally, the growth rates for P3 and P4 were nearly the same, at 69 and 78 days, respectively (Fig. 1). The tumor growth rate downregulation were corelated the NK cell mediated cytotoxicity activity (Fig. 4). This observation suggests that athymic nude mice model lacks functional T cells but still has NK cells, which are part of the innate immune system and play a role in immune surveillance against tumors. These effects, however, may vary due to factors such as the ability of tumors to evade host immune detection or the influence of the tumor microenvironment on NK cell activity. NK cells from the athymic nude mice can recognize and kill tumor cells through various mechanisms, including direct cytotoxicity and the secretion of cytokines, such as INF-γ[19]. After PDX passages, NK cells in athymic nude mice may still exert some level of cytotoxicity against the transplanted human tumor cells. However, the

extent of this cytotoxicity may vary depending on several factors. Firstly, NK cells in athymic nude mice may be more effective at recognizing and killing tumor cells during the initial PDX passage from P0 to P1 than in subsequent passages. This could limit their impact on PDX tumor growth, as observed in our PDX model at P0. Secondly, tumors often employ mechanisms to evade host immune detection and destruction, including resistance to NK cell-mediated cytotoxicity. This can involve the downregulation of ligands for NK cell activating receptors or the upregulation of inhibitory signals, such as NEAT1 and MALAT1 lncRNAs (Fig. 6). Thirdly, the tumor microenvironment within PDX models may influence the activity of NK cells. Factors such as hypoxia, immune cell infiltrates, and interactions with stromal cells can modulate NK cell function[20,21]. The RT-qPCR data presented were derived from triplicate experiments, leading us to believe that the observed differences are not due to technical errors (Fig. 6). We hypothesize that human MALAT1, compared to mouse Malat1, plays a more significant role in the context of PDX models, particularly in terms of host immunoregulation. This differential expression is likely influenced by species-specific regulatory mechanisms, which merit further investigation.

Long non-coding RNAs, over 200 nucleotides in length, are a class of transcripts without amino acid-coding potential, which impact molecular and cellular processes, including gene regulation, ligand-receptor activity, and cellular signaling, thereby playing fundamental roles in various physiological and pathological processes[22–24]. NEAT1 and MALAT1 are among the most well-studied lncRNAs, and they are indeed highly abundant in the nucleus of cells. NEAT1 and MALAT1 are dysregulated and elevated in various types of cancers[22–24].

NEAT1 plays a role in forming and maintaining nuclear paraspeckles, which are subnuclear bodies that regulate gene expression. NEAT1 acts as a competing lncRNA to sponge tumor-suppressive microRNAs to mediate tumor progression[18,24]. Upregulation of NEAT1 has been implicated in the progression of several cancers as an oncogene, including lung cancer, esophageal cancer, colorectal cancer, breast cancer, prostate cancer, and pancreatic cancer[25]. On the contrary, NEAT1 downregulation contributes to the blockade of differentiation in acute leukemia as a tumor suppressor[26]. The dysregulation of NEAT1 and MALAT1 in cancer suggests that they may play essential roles in tumor development and progression. They have been implicated in various aspects of cancer biology, including cell proliferation, survival, migration, invasion, and resistance to therapy. As discussed earlier, emerging evidence suggests that NEAT1 and MALAT1 may also influence the tumor microenvironment, including immune cell infiltration. Therefore, targeting NEAT1 and MALAT1 could potentially be a strategy for cancer therapy, and they are also being investigated as potential biomarkers for cancer diagnosis, prognosis, and prediction of therapeutic response. LncRNA NEAT1 has been implicated in regulating various cellular processes, including cell proliferation, in different cell types, including NK cells[17]. While there is limited specific research on the direct involvement of NEAT1 in NK cells cytotoxicity signal pathways, some studies suggest its potential role in modulating immune responses[24,27,28]. Studies have shown that NEAT1 plays a role in modulating the proliferation, apoptosis, cell cycle and activation of NK cells[29]. NEAT1 expression has been found to be upregulated during NK cell activation, and its knockdown has been shown to suppress NK cell proliferation and cytotoxicity[30]. Additionally, NEAT1 has been implicated in regulating the expression of genes involved in NK cell function, such as genes encoding cytokines and cytotoxic molecules. Through its interactions with proteins and other RNAs, NEAT1 likely contributes to the intricate regulatory network that governs NK cell proliferation and function[29]. The impact of NEAT1 on PDX model generation would likely depend on its role in tumorigenesis and tumor progression[31]. In our findings, NEAT1 promotes tumor growth or metastasis; manipulating its expression in patient-derived tumor cells before implantation into nude mice could potentially affect tumor engraftment and growth in the PDX model. Additionally, NEAT1 may influence the tumor microenvironment, including immune cell infiltration and activity[32], which could also affect PDX model development and characteristics.

The lncRNA MALAT1 was first found as a metastasis-associated lung adenocarcinoma transcript that has been implicated in various cellular processes, including gene regulation, chromatin organization, and RNA processing[33]. While their roles in cancer progression and metastasis have been extensively studied, their involvement in immune cell infiltration is an emerging area of research[23]. Recent studies have suggested that NEAT1 as a competing endogenous RNA in tumorigenesis of various cancer may influence immune cell infiltration within the tumor microenvironment[24]. MALAT1 and NEAT1 are the lncRNAs in the competing endogenous RNAs (ceRNAs) networks that regulate other RNA transcripts by competing for shared microRNAs (miRNAs). NEAT1 and MALAT1 participated in the immune cell infiltration in bladder cancer[18].

Athymic nude mice retain NK cell-mediated cytotoxic activity. Eat-2 is an Src homology 2 domain-containing intracellular adaptor expressed in NK cells that aids in the elimination of abnormal or foreign cells[34]. Mouse klrd1, also known as CD94, clusters with Nkg2d in NK cells to mediate immune responses[35]. Mouse β2 integrin (also known as CD18) is part of a family of integrin proteins that play critical roles in immune cell adhesion, migration, and signaling. These integrins form heterodimers with various alpha integrin subunits, resulting in different functional integrins such as lymphocyte function-associated antigen (LFA-1) with any of the activating receptors[36]. In NK cells, β2 integrins, particularly LFA-1, mediate cell adhesion to target cells, synapse formation, and cytotoxicity[37]. Increased expression of β2 integrin and the Klrd1/Nkg2d complex in athymic nude mice could potentially enhance NK cell cytotoxicity by improving their ability to adhere to and form synapses with target cells, leading to more effective killing. This could be a significant factor in studying immune cell interactions and cancer progression in the PDX athymic nude model. There is evidence suggesting that NEAT1 and MALAT1 lncRNAs can influence β2 integrin expression, though the exact mechanisms are still being explored.

Establishing PDX models is a time-consuming yet essential process for accurately replicating the human tumor microenvironment, crucial for advancing translational medicine approaches. In our study, we utilized bioinformatics analysis to identify the functional roles of lncRNAs NEAT1 and MALAT1 within these models. This approach allowed us to elucidate the molecular immune mechanisms that may regulate tumor growth,

highlighting the potential involvement of these lncRNAs. However, our study confronts inherent limitations, notably the absence of direct wet lab experimental evidence, a common challenge in bioinformatics-based research. The next phase would be employing advanced molecular cell biology techniques for direct assessments to address these gaps and build upon our preliminary findings. These investigations are anticipated to enrich our understanding of the roles PDX models play in the growth of lung adenocarcinoma and the specific contributions of lncRNAs NEAT1 and MALAT1 to immune regulation.

Conclusions

In conclusion, the PDX model using athymic nude mice offers a promising platform for exploring the complexities of tumor-immune dynamics. This study provides novel insights into the roles of NK cells and regulatory lncRNAs, such as NEAT1 and MALAT1, in modulating tumor growth. These findings lay a foundation for future research aimed at enhancing the effectiveness of cancer therapies. Understanding these interactions allows for more tailored interventions that leverage the body's immune response while countering tumor resistance mechanisms.

Data availability

Data supporting the findings of this study are provided within the manuscript and its supplementary information files. Additionally, the RNA sequencing datasets generated during the current study using Illumina sequencing are publicly available in the NCBI Gene Expression Omnibus (GEO) under accession number GSE295073.

Received: 5 September 2024; Accepted: 30 May 2025
Published online: 02 July 2025

References

1. Siegel, R. L. et al. Cancer statistics, 2022. *CA Cancer J. Clin.* **72** (1), 7–33 (2022).
2. Jones, G. S. & Baldwin, D. R. Recent advances in the management of lung cancer. *Clin. Med. (Lond).* **18** (Suppl 2), s41–s46 (2018).
3. Gao, H. et al. High-throughput screening using patient-derived tumor xenografts to predict clinical trial drug response. *Nat. Med.* **21** (11), 1318–1325 (2015).
4. Hidalgo, M. et al. Patient-derived xenograft models: an emerging platform for translational cancer research. *Cancer Discov.* **4** (9), 998–1013 (2014).
5. Drapkin, B. J. et al. Genomic and functional fidelity of small cell lung Cancer Patient-Derived xenografts. *Cancer Discov.* **8** (5), 600–615 (2018).
6. Fichtner, I. et al. Establishment of patient-derived non-small cell lung cancer xenografts as models for the identification of predictive biomarkers. *Clin. Cancer Res.* **14** (20), 6456–6468 (2008).
7. Kita, K. et al. Patient-derived xenograft models of non-small cell lung cancer for evaluating targeted drug sensitivity and resistance. *Cancer Sci.* **110** (10), 3215–3224 (2019).
8. Zhao, L. et al. Targeted radionuclide therapy in Patient-Derived xenografts using (177)Lu-EB-RGD. *Mol. Cancer Ther.* **19** (10), 2034–2043 (2020).
9. Fiebig, H. H. et al. Development of three human small cell lung cancer models in nude mice. *Recent. Results Cancer Res.* **97**, 77–86 (1985).
10. Chen, X. et al. Patient-derived non-small cell lung cancer xenograft mirrors complex tumor heterogeneity. *Cancer Biol. Med.* **18** (1), 184–198 (2021).
11. Sherman, B. T. et al. DAVID: a web server for functional enrichment analysis and functional annotation of gene lists (2021 update). *Nucleic Acids Res.* **50** (W1), W216–W221 (2022).
12. Kanehisa, M. & Goto, S. KEGG: Kyoto encyclopedia of genes and genomes. *Nucleic Acids Res.* **28** (1), 27–30 (2000).
13. Kanehisa, M. et al. KEGG for taxonomy-based analysis of pathways and genomes. *Nucleic Acids Res.* **51** (D1), D587–D592 (2023).
14. Kanehisa, M. Toward Understanding the origin and evolution of cellular organisms. *Protein Sci.* **28** (11), 1947–1951 (2019).
15. Crozat, K. et al. Impact of beta2 integrin deficiency on mouse natural killer cell development and function. *Blood* **117** (10), 2874–2882 (2011).
16. Kim, S. H. et al. Association of the long non-coding RNA MALAT1 with the polycomb repressive complex pathway in T and NK cell lymphoma. *Oncotarget* **8** (19), 31305–31317 (2017).
17. Wang, Q. M. et al. Exosomal LncRNA NEAT1 inhibits NK cell activity to promote multiple myeloma cell immune escape via an EZH2/PBX1 axis. *Mol. Cancer Res.* (2023).
18. Rao, X. et al. NEAT1/MALAT1/XIST/PKD–Hsa-Mir-101-3p–DLGAP5 Axis as a novel diagnostic and prognostic biomarker associated with immune cell infiltration in bladder Cancer. *Front. Genet.* **13**, 892535 (2022).
19. Kim, J. S. et al. Inhibition of human pancreatic tumor growth by cytokine-induced killer cells in nude mouse xenograft model. *Immune Netw.* **12** (6), 247–252 (2012).
20. Liu, Y. et al. Patient-derived xenograft models in cancer therapy: technologies and applications. *Signal. Transduct. Target. Ther.* **8** (1), 160 (2023).
21. Melaiu, O. et al. Influence of the tumor microenvironment on NK cell function in solid tumors. *Front. Immunol.* **10**, 3038 (2019).
22. Klopotowska, D. & Matuszyk, J. Downregulation of MALAT1 in triple-negative breast cancer cells. *Biochem. Biophys. Rep.* **37**, 101592 (2024).
23. Schmidt, L. H. et al. The long noncoding MALAT-1 RNA indicates a poor prognosis in non-small cell lung cancer and induces migration and tumor growth. *J. Thorac. Oncol.* **6** (12), 1984–1992 (2011).
24. Li, K. et al. NEAT1 as a competing endogenous RNA in tumorigenesis of various cancers: role, mechanism and therapeutic potential. *Int. J. Biol. Sci.* **17** (13), 3428–3440 (2021).
25. Yu, X. et al. NEAT1: A novel cancer-related long non-coding RNA. *Cell. Prolif.* **50** (2) (2017).
26. Zeng, C. et al. Inhibition of long non-coding RNA NEAT1 impairs myeloid differentiation in acute promyelocytic leukemia cells. *BMC Cancer.* **14**, 693 (2014).
27. Gu, J. et al. Molecular interactions of the long noncoding RNA NEAT1 in cancer. *Cancers (Basel)* **14** (16) (2022).
28. Guo, F. et al. Downregulation of the long non-coding RNA MALAT1 in tenofovir-treated pregnant women with hepatitis B virus infection promotes immune recovery of natural killer cells via the has-miR-155-5p/HIF-1alpha axis. *Int. Immunopharmacol.* **107**, 108701 (2022).
29. Yang, C. et al. Noncoding RNA in NK cells. *J. Leukoc. Biol.* **105** (1), 63–71 (2019).
30. Pan, Y. et al. Novel insights into the emerging role of Neat1 and its effects downstream in the regulation of inflammation. *J. Inflamm. Res.* **15**, 557–571 (2022).
31. Hussain, M. S. et al. Exploring the role of Lncrna neat1 knockdown in regulating apoptosis across multiple cancer types: A review. *Pathol. Res. Pract.* **252**, 154908 (2023).

32. Toker, J. et al. Clinical importance of the LncRNA NEAT1 in Cancer patients treated with immune checkpoint inhibitors. *Clin. Cancer Res.* **29** (12), 2226–2238 (2023).
33. Song, J., Su, Z. Z. & Shen, Q. M. Long non-coding RNA MALAT1 regulates proliferation, apoptosis, migration and invasion via miR-374b-5p/SRSF7 axis in non-small cell lung cancer. *Eur. Rev. Med. Pharmacol. Sci.* **24** (4), 1853–1862 (2020).
34. Perez-Quintero, L. A. et al. EAT-2, a SAP-like adaptor, controls NK cell activation through phospholipase cgamma, Ca++, and Erk, leading to granule polarization. *J. Exp. Med.* **211** (4), 727–742 (2014).
35. Ho, E. L. et al. Murine Nkg2d and Cd94 are clustered within the natural killer complex and are expressed independently in natural killer cells. *Proc. Natl. Acad. Sci. U S A.* **95** (11), 6320–6325 (1998).
36. Barber, D. F., Faure, M. & Long, E. O. LFA-1 contributes an early signal for NK cell cytotoxicity. *J. Immunol.* **173** (6), 3653–3659 (2004).
37. Urlaub, D. et al. LFA-1 activation in NK cells and their subsets: influence of receptors, maturation, and cytokine stimulation. *J. Immunol.* **198** (5), 1944–1951 (2017).

Acknowledgements
We greatly appreciate technical support from the Core Laboratory of the Taipei Tzu Chi Hospital, Buddhist Tzu Chi Medical Foundation. The KEGG project is partially supported by the National Bioscience Database Center of the Japan Science and Technology Agency.

Author contributions
M. H., M. L., B. H., and J. H. contributed to the conceptualization of the manuscript. M. L. and B. H. were responsible for data collection and statistical analysis. B. H. drafted the initial manuscript. M. H. and J. H. performed manuscript revisions. J. H. also managed the acquisition of research funding and supervised the project. All authors have read and agreed to the published version of the manuscript.

Funding
This work was funded by Tzu Chi University (TCAS-110-02 and TCAS-112-04), the National Science and Technology Council (109-2314-B-038-039 and 110-2314-B-303-013-MY3), Taipei Tzu Chi Hospital, Buddhist Tzu Chi Medical Foundation (TCRD-TPE-112-04, TCRD-TPE-MOST-109-03, TCRD-TPE-MOST-112-15).

Declarations

Competing interests
The authors declare no competing interests.

Ethical approval
The Institutional Review Board of Taipei Tzu Chi General Hospital, Buddhist Tzu Chi Medical Foundation reviewed and approved the human tumor specimen protocol (Approval number: IRB 10-XD-104); the Institutional Animal Care and Use Committee of Taipei Tzu Chi General Hospital, Buddhist Tzu Chi Medical Foundation reviewed and approved the animal experiment protocol (Approval number: 110-IACUC-016). All animal handling and experiments strictly followed the ARRIVE guidelines for animal research and reporting for in vivo experiments. All methods were performed in accordance with the relevant guidelines and regulations.

Additional information
Supplementary Information The online version contains supplementary material available at https://doi.org/10.1038/s41598-025-05157-z.

Correspondence and requests for materials should be addressed to B.-Y.H. or J.-K.H.